CRYSTALLOGRAPHY REPORTS, 2025, Vol. 70, No. 1, pp. 115–120

NANOMATERIALS, CERAMICS

COMPUTER SIMULATION OF AGI|SI_3O_6 COMPLEX NANOCOMPOSITES IN SINGLE-WALL CARBON NANOTUBES

© 2025 A. V. Petrov[a,*], I. V. Murin[a], and A. K. Ivanov-Schitz[b]

[a] Saint Petersburg State University, Saint Petersburg, Russia
[b] Shubnikov Institute of Crystallography, Kurchatov Complex of Crystallography and Photonics, National Research Centre "Kurchatov Institute", Moscow, Russia
*e-mail: a.petrov@spbu.ru

Received June 26, 2024
Revised August 19, 2024
Accepted August 19, 2024

Abstract. The method of molecular dynamics has been used to simulate heteronanostructures formed when silver iodide and silicon oxide nanoparticles are filling single-walled carbon nanotubes of the "armchair" type (12, 12). The results of computer modeling show that stable nanostructured "internal nanocomposites" with AgI inclusions and silicon oxide clusters of various configurations can be formed in such tubes. Si_3O_6 clusters of linear and planar types have varying degrees of influence on the mobility of silver ions in the studied complex heteronanostructures of AgI|Si_3O_6@SWCNT.

DOI: 10.31857/S00234761250116e4

INTRODUCTION

Among nanomaterials, particularly composite ones, nanocrystalline structures composed of inorganic clusters distributed within a crystalline, glassy, or polymorphic matrix or filling nanotubes of various compositions and properties (single-walled, multi-walled, with different chirality and lengths, etc.) are of particular interest [1–8]. A significant body of research is dedicated to inorganic nanostructures formed within carbon nanotubes (**CNT**) [9–15]. CNT, including those in nanocomposites, are widely used in various solid-state electrochemical devices as electrode materials [16–18], both as anodes [19–21] and cathodes [22].

Alongside experimental methods for studying nanostructures (high-resolution transmission electron microscopy, Raman spectroscopy, etc.), computational modeling techniques such as molecular statics, molecular dynamics, and Monte Carlo methods are actively employed. These approaches allow for the calculation of structural and energetic characteristics as well as the dynamic properties (mass and charge transport) of the studied nanosystems [23–26].

Classical molecular dynamics (**MD**) simulations have been used to study the formation of nanocrystalline structures in single-walled carbon nanotubes (**SWCNT**) and the properties of the resulting nanocomposite systems [26–29].

Previous studies have investigated model structures of Ag*X*@SWCNT (*X* = I, Br) [30–33] and SnF_2@SWCNT [34]. It has been shown that silver iodide nanostructures in SWCNT can adopt nanotubular structures based on a hexagonal lattice; however, in some cases, AgI nanotubes based on a square lattice were also observed. The AgI@SWCNT heterostructures exhibit lower silver ion diffusion coefficients compared to bulk silver iodide. For SWCNT filled with silver bromide, the formation of nanotubes based on either a square or hexagonal lattice, as well as fragments of a bulk NaCl-type structure, was observed. In the SnF_2@SWCNT system, model CNT of different sizes reproduced both an ordered structure in the form of an internal SnF_2 nanotube and a significantly disordered (glassy) phase. Upon heating the SnF_2@SWCNT model system, a state characterized by noticeable fluoride ion mobility was observed. The effect of changes (both increases and decreases) in ionic conductivity in two-phase composite systems is well known [35], and in [36], an increase in ionic conductivity of fluoride-conducting solid solutions was demonstrated upon the addition of inert silicon oxide particles.

The aim of this study is to model the formation processes of complex heterostructures consisting of AgI|Si_3O_6 nanostructures inside SWCNT and to determine the structural and dynamic characteristics of the resulting systems.

SIMULATED SYSTEM DESCRIPTION

Obtaining a complex composite material based on nanotubes with simultaneous filling by silver iodide and silicon oxide is complicated by the significant difference in their melting temperatures. Therefore, we propose introducing pre-formed Si_3O_6 clusters into the nanotubes.

Silicon oxide SiO_2 can be represented as a Si_3O_6 nanocluster. However, as shown in our previous studies, selecting the shape of even such a cluster is not a straightforward task. *Ab initio* calculations were used to determine the charge states and optimized equilibrium geometries [37, 38] of two different types of Si_3O_6 nanoclusters – linear and planar (Fig. 1).

The calculated electronic and structural characteristics of the linear and planar Si_3O_6 nanocluster forms were then used for co-filling SWCNTs with silver and iodide ions to model the dynamic properties of the composite material inside the nanotube.

Molecular dynamics (MD) simulations were performed using the Forcite module in Materials Studio to characterize the structural and dynamic properties of the investigated systems [39].

In the preliminary stage of the study, it was shown that the type of carbon nanotube ("zigzag" or "armchair") has a minor effect on nanocomposite formation. Therefore, we selected armchair-type SWCNTs (12,12) with a diameter of 16.27 Å. The creation of SWCNTs and their filling with atoms, molecules, and particles is a standard procedure in the Materials Studio package [39]. In the generated SWCNT, which had a length of 40 Å, 30 precomputed Si_3O_6 nanoparticles, either in linear or planar form (without mixed filling), were randomly distributed. In the next step, the nanotube was additionally filled with I^- (charge: $-0.79e$) and Ag^+ (charge: $+0.79e$) ions in a stoichiometric ratio. This procedure was carried out using the Amorphous Cell module in Materials Studio, where the ions were placed randomly, but placement near the inner surface of the nanotube (~3 Å) was prohibited. The number of silver and iodide ions was determined based on the estimated composite density of 5.5 g/cm^3. The SWCNT filled with AgI and Si_3O_6 was then placed in a simulation cell with periodic boundary conditions.

For MD calculations, we used interatomic potentials of the Universal Force Field type. Ion charges were computed using quantum chemical methods. The simulations were performed in the NVT ensemble using a Nosé–Hoover thermostat, with a time step of 0.1 fs (10^{-16} s) and simulation durations of up to 100 ps (for some control simulations, up to 1 ns). The temperature range varied from room temperature to the melting point.

Radial distribution functions (RDFs) were calculated to analyze structural features of the simulated system:

$$g_{ij}(r) = \frac{n_{ij}(r)}{\rho \cdot 4\pi r^2 dr}, \quad (1)$$

where n is the average number of j-type particles in a spherical shell of thickness dr at a distance r from an i-type particle, and ρ is the average atomic density of the modeled system.

Particle mobility was characterized using mean square displacement (**MSD**) functions:

$$\langle r^2(t) \rangle = \frac{1}{N}\sum_{k=1}^{N}\Big(\big[x_k(t) - x_k(0)\big]^2 + \big[y_k(t) - y_k(0)\big]^2 + \big[z_k(t) - z_k(0)\big]^2\Big), \quad (2)$$

where $x_k(t)$, $y_k(t)$ and $z_k(t)$ are the coordinates of the k-th particle at time t. The time dependence of MSD (except for the initial segment) was approximated by linear functions, and the diffusion coefficients of the ions (D) were calculated from the slope of the linear fit using Einstein's relation:

$$r^2(t) = 6Dt + B, \quad (3)$$

where the coefficient B accounts for thermal vibrations of particles around their equilibrium positions.

SYSTEM SIMULATION AND RESULTS

Structural characteristics. Figs. 2 and 3 schematically show the structures of the obtained AgI|Si_3O_6@SWCNT (12,12) composites. It is evident that introducing Si_3O_6 silicon oxide nanoparticles of different shapes into the nanotube leads to different realizations of the complex nanocomposite state inside the CNT.

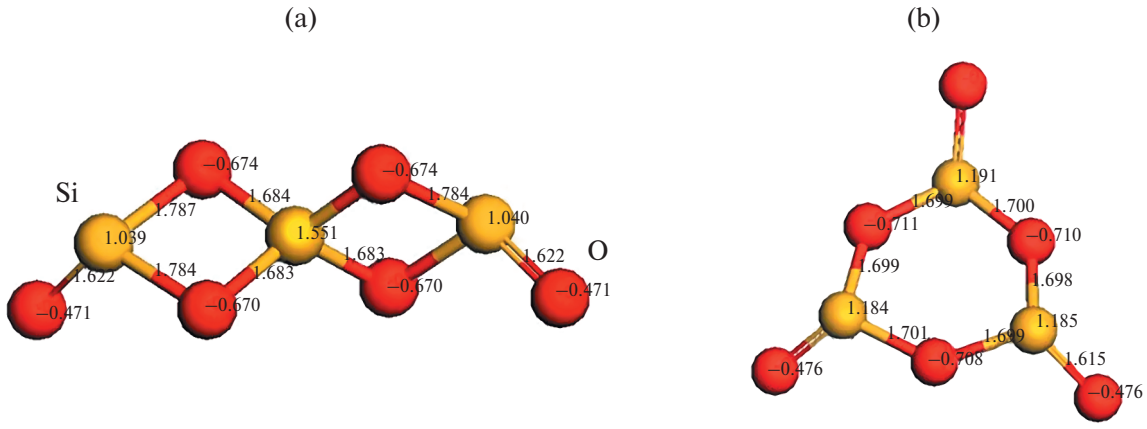

Fig. 1. Bond lengths and charge states of the linear (a) and planar (b) forms of Si_3O_6 nanoparticles.

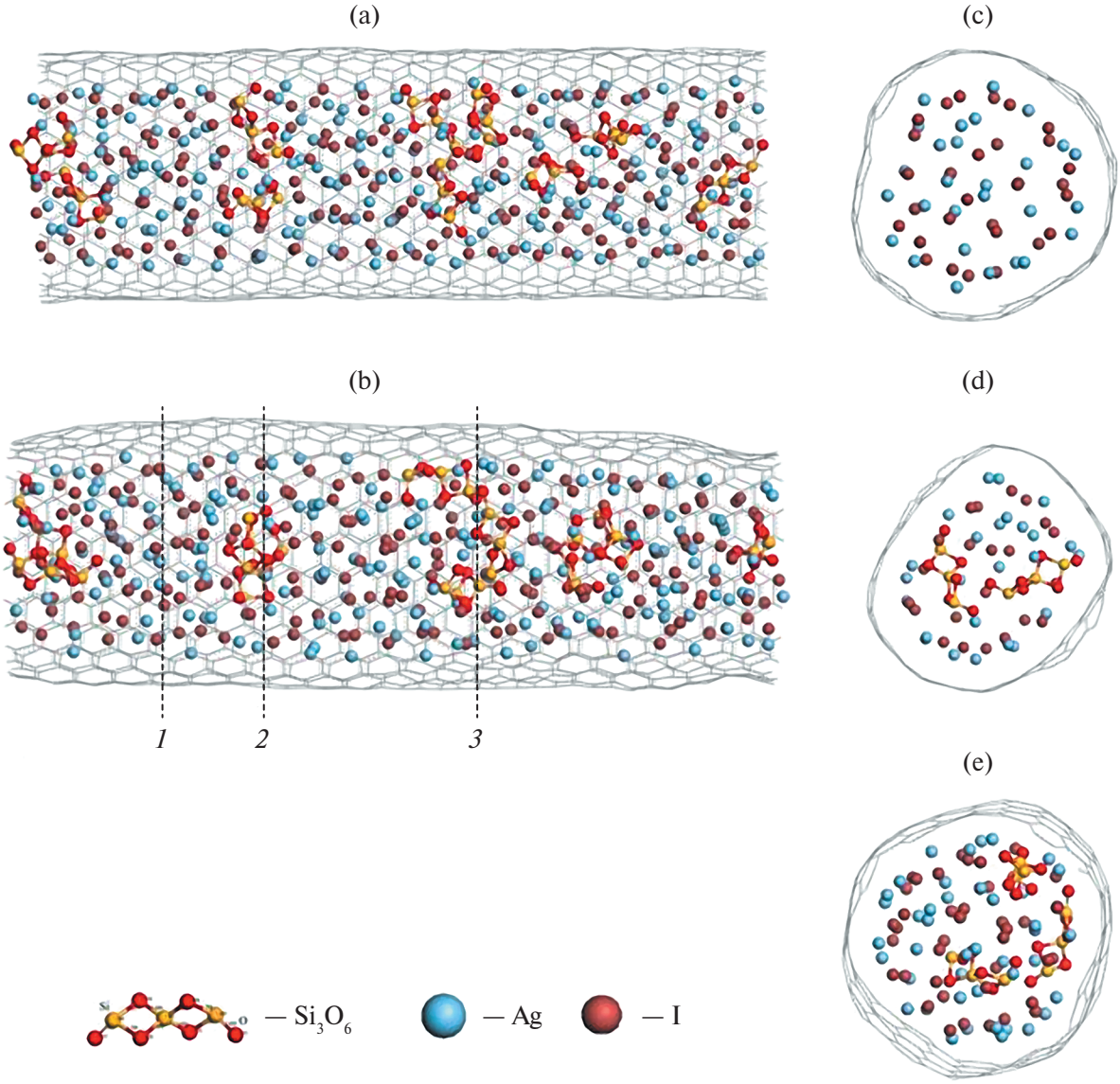

Fig. 2. Longitudinal (initial (a) and final (b) states) and cross-sections (c–e) of SWCNT filled with silver iodide and linear Si_3O_6 nanoparticles. Calculations at 900 K; cross-sections represent a layer 12–15 Å thick; numbers in Fig. b indicate cross-sections in Fig. c–e.

As seen in Figs. 2a, 2b, 3a, and 3b, the calculations show slight deformation of the nanotubes and significant redistribution of Ag and I atoms, while the silicon oxide nanoclusters undergo only minor distortions and displacements. Furthermore, despite the initial random spatial distribution of Si_3O_6 particles inside the nanotubes, "empty" and "densely packed" regions with nanoparticle agglomerates are observed. Analyzing the distribution of silicon oxide particles in cross-sections of different regions (Figs. 2, 3c–3e) suggests that even in the densely packed areas, there remains sufficient free space for the possible transport of Ag and I ions.

Fig. 4 presents the RDF of different ion pairs at 900 K as an example. The RDF analysis for AgI inside the nanotube showed that the shape of the silicon oxide nanoclusters does not significantly affect the distribution of silver and iodide ions within the nanotube. The only notable change is in *g(r)* for silver–silver pairs, with peak broadening indicating the high mobility of the cationic subsystem.

Notably, as the temperature increases, the general shape of the RDF remains unchanged, with only peak broadening and a slight rightward shift of peak maxima due to thermal expansion. This suggests that at low temperatures, silver iodide forms chain-like structures in a disordered silver phase, followed by the "amorphization" of AgI, where both ion types exhibit relatively high mobility, although silver cations are more mobile. To confirm this hypothesis, we analyzed the dynamic characteristics of the AgI|Si_3O_6 nanocomposite components.

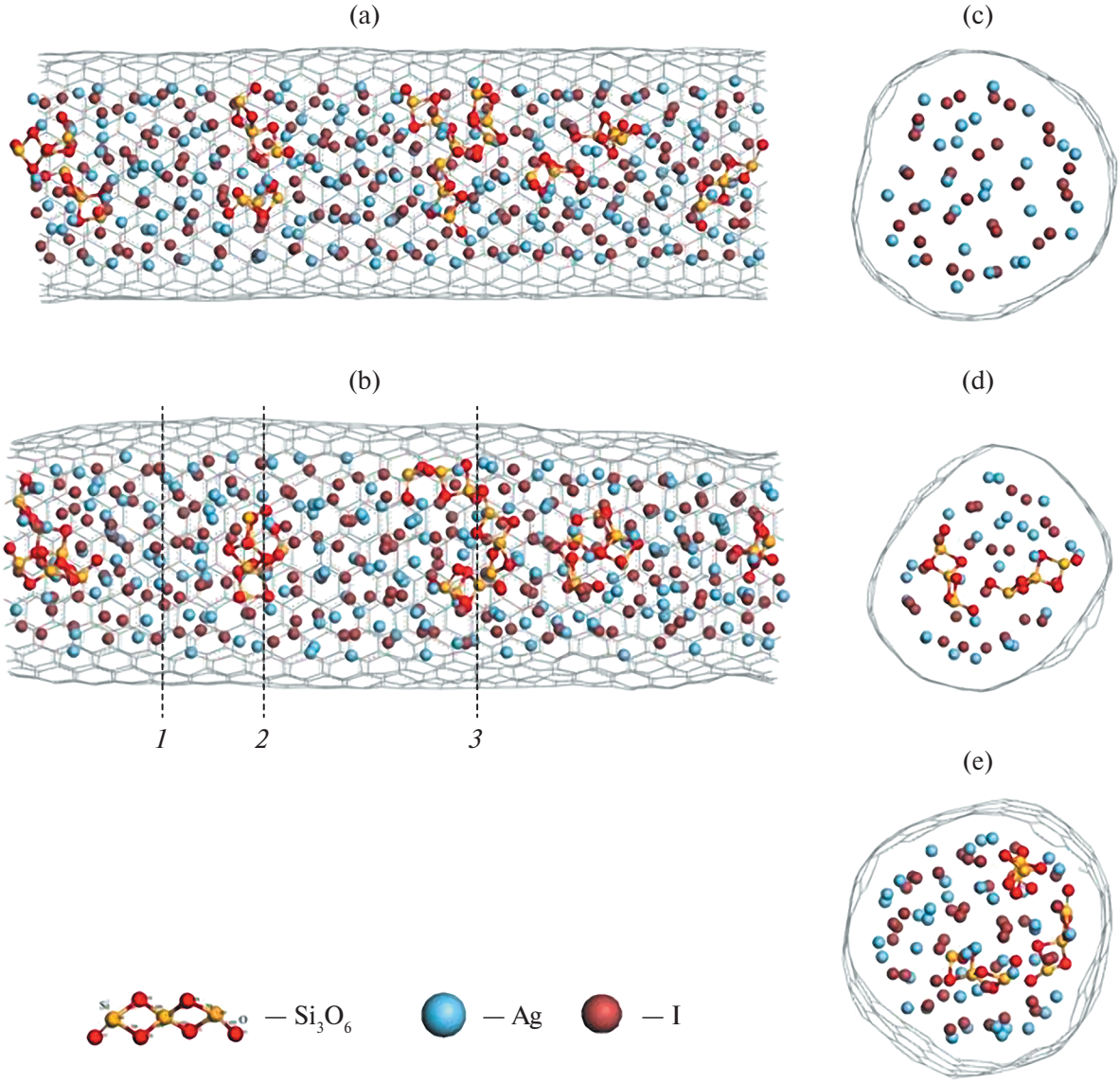

Fig. 3. Longitudinal (initial (a) and final (b) states) and cross-sections (c–e) of SWCNT filled with silver iodide and planar Si_3O_6 nanoparticles. Calculations at 900 K; cross-sections represent a layer with a thickness of 12–15 Å; numbers in Fig. b indicate sections in Fig. c–e.

Dynamic characteristics. To evaluate the mobility of silver and iodide ions, we examined the time dependence of MSD, shown in Fig. 5 for 900 K as an example.

The MSD slopes indicate that silver cations exhibit the highest mobility in nanotubes containing planar Si_3O_6 particles. The calculated diffusion coefficients of silver and iodide ions for structures with different Si_3O_6 cluster types are presented in Fig. 6. For comparison, the diffusion coefficients of Ag^+ and I^- in a SWCNT without silicon oxide nanoparticles are also shown [31]. The data in Fig. 6 suggest that silver iodide melts at approximately 800–900 K, whereas in a "pure" nanotube, no melting of AgI is observed. However, the presence of Si_3O_6 nanoparticles reduces the diffusion coefficients of silver and iodide by about an order of magnitude.

The MSD analysis, along with the results in Figs. 2 and 3, indicates that Si_3O_6 nanoclusters primarily undergo "rotational-translational" motion as a whole, with little evidence of significant translational movement.

Thus, by varying the concentration and type of Si_3O_6 nanoclusters, it is possible to significantly control the mobility of silver ions in the AgI|Si_3O_6@SWCNT heterostructure.

CONCLUSION

The conducted computer modeling indicates that for a 40 Å long SWCNT (12,12) with silver iodide inclusions, stable nanostructured "internal nanocomposites" are formed, incorporating Si_3O_6

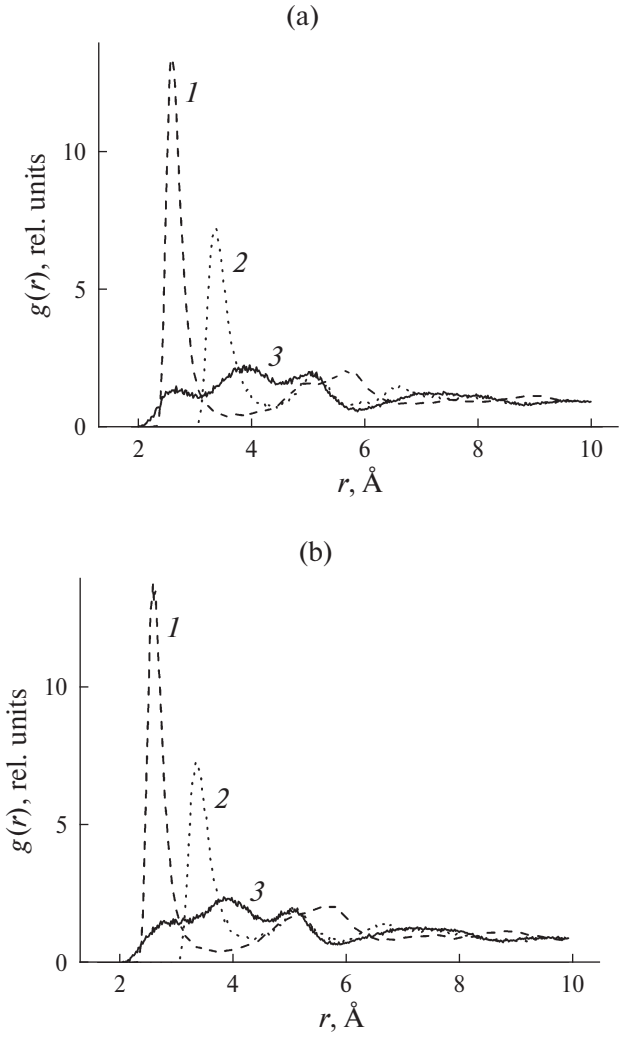

Fig. 4. RDFs of Ag–I (*1*), I–I (*2*) and Ag–Ag (*3*) pairs in tubes with linear (a) and planar (b) nanoclusters at 900 K.

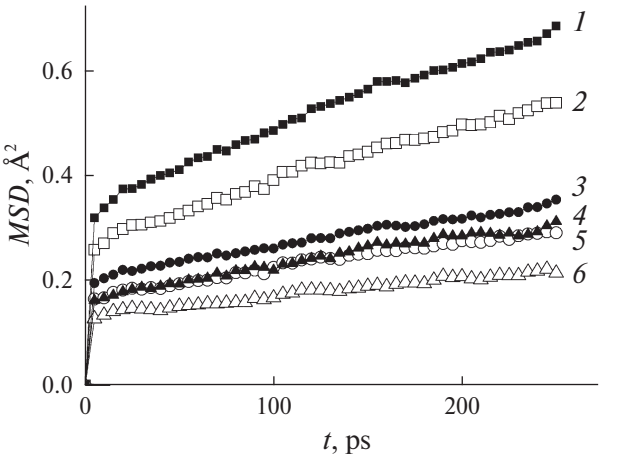

Fig. 5. Time dependences of the *MSD* of ions in tubes filled with Si_3O_6 nanoparticles of planar (*1* – Ag, *3* – I, *4* – Si) and linear (*2* – Ag, *5* – I, *6* – Si) forms (at 900 K).

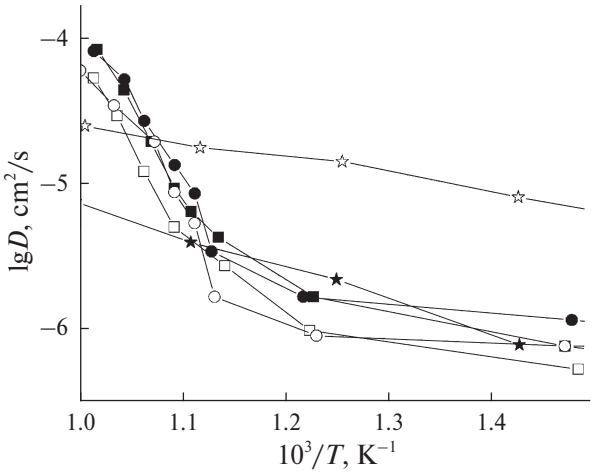

Fig. 6. Diffusion of silver and iodine ions in tubes: ■ – Ag in SWCNT with a linear Si_3O_6 cluster, □ – I in SWCNT with a linear Si_3O_6 cluster, • – Ag in SWCNT with a planar Si_3O_6 cluster, ○ – I in SWCNT with a linear Si_3O_6 cluster, ☆ – Ag in SWCNT (11,11) [31], ★ – I in SWCNT (11,11) [31].

silicon oxide clusters of various configurations – linear and planar. These complexly organized composites can transition into a state with quasi-molten (amorphous) "chains" of silver iodide. The obtained results confirm the possibility of controlling high ionic conductivity in complex AgI|Si_3O_6@SWCNT heteronanostructures by selecting both the shape and concentration of silicon oxide nanoclusters.

FUNDING

This work was carried out as part of the 2024 SPbU initiative project No. 116881298 using the computational resources of the Resource Center "Computing Center of SPbU" (http://cc.spbu.ru) and under the State Assignment of the NRC "Kurchatov Institute".

CONFLICT OF INTERESTS

The authors declare no conflict of interest.

REFERENCES

1. *Mekuye B., Abera B.* // Nano Select. 2023. V. 4. P. 486. https://doi.org/10.1002/nano.202300038
2. *Baig N., Kammakakam I., Falath W.* // Mater. Adv. 2021. V. 2. P. 1821. https://doi.org/ 10.1039/d0ma00807a
3. *Saleh H.M., Hassan A.I.* // Sustainability. 2023. V. 15. No. 14. P. 10891. https://doi.org/10.3390/su151410891
4. *Rizvi M., Gerengi H., Gupta P.* // ACS Symp. Ser. 2022. V. 1418. P. 1. https://doi.org/10.1021/bk-2022-1418.ch001

5. *Rao R., Pint C.L., Islam A.E. et al.* // ACS Nano. 2018. V. 12. P. 11756. https://doi.org/10.1021/acsnano.8b06511
6. *Zhang Y., Rhee K.Y., Hui D. et al.* // Compos. B. Eng. 2018. V. 143. P. 19. https://doi.org/10.1016/j.compositesb.2018.01.028
7. *Jadoun S., Chauhan N.P.S., Chinnam S. et al.* // Biomedical Materials Devices. 2023. V. 1. P. 351. https://doi.org/10.1007/s44174-022-00009-0
8. *Barbaros I., Yang Y., Safaei B. et al.* // Nanotechnol. Rev. 2022. V. 11. P. 321. https://doi.org/10.1515/ntrev-2022-0017
9. *Ilie A., Crampin S., Karlsson L., Wilson M.* // Nano Res. 2012. V. 5. P. 833. https://doi.org/10.1007/s12274-012-0267-5
10. *Eatemadi M., Daraee H., Karimkhanloo H. et al.* // Nanoscale Res. Let. 2014. V. 9. P. 393. https://doi.org/10.1186/1556-276X-9-393
11. *Rakhi R.B.* // Nanocarbon and its Composites / Eds. Khan A. et al. Woodhead Publishing, 2019. 489 p. https://doi.org/10.1016/B978-0-08-102509-3.00016-X
12. *Sandoval S., Tobias G., Flahaut E.* // Inorganica Chim. Acta. 2019. V. 492. P. 66. https://doi.org/10.1016/j.ica.2019.04.004
13. *Ates M., Eker A.A., Eker B.* // J. Adhesion Sci. Technol. 2017. V. 31. P. 1. https://doi.org/10.1080/01694243.2017.1295625
14. *Poudel Y.R., Li W.* // Mater. Today Phys. 2018. V. 7. P. 74. https://doi.org/10.1016/j.mtphys.2018.10.002
15. *Kharlamova M.V., Kramberger C.* // Nanomaterials. 2021. V. 11. P. 2863. https://doi.org/10.3390/nano11112863
16. *Li L., Yang H., Zhou D. et al.* // J. Nanomater. 2014. V. 2014. Art. 187891. https://doi.org/10.1155/2014/187891
17. *Nwanno C.E., Li W.* // Nano Res. 2023. V. 16. P. 12384. https://doi.org/10.1007/s12274-023-6006-2
18. *Xiong J.Z., Yang Z.C., Guo X.L. et al.* // Tungsten. 2024. V. 6. P. 174. https://doi.org/10.1007/s42864-022-00177-y
19. *Zhang D., Ye Z., Liu Z. et al.* // Energy Storage Sci. Technol. 2023. V. 12. P. 2095. https://doi.org/10.19799/j.cnki.2095-4239.2023.0178
20. *Hou Z.-d., Gao Y.-y., Zhang Y. et al.* // New Carbon Mater. 2023. V. 38. P. 230. https://doi.org/10.1016/S1872-5805(23)60725-5
21. *Thauer E., Ottmann A., Schneider P. et al.* // Molecules. 2020. V. 25. P. 1064. https://doi.org/10.3390/molecules25051064
22. *Babkin A.V., Kubarkov A.V., Drozhzhin O.A. et al.* // Dokl. Chem. 2023. V. 508. P. 1. https://doi.org/10.1134/S001250082360013X
23. *Enyashin A.N.* // Comput. Mater. Discovery. 2018. P. 352. https://doi.org/10.1039/9781788010122-00352
24. *Shunaev V.V., Petrunin A.A., Zhan H. et al.* // Materials. 2023. V. 16. P. 3270. https://doi.org/10.3390/ma16083270.
25. *Zare Y., Yop Rhee K., Park S.-J.* // Results Phys. 2019. V. 15. P. 102562. https://doi.org/10.1016/j.rinp.2019.102562
26. *Vivanco-Benavides L.E., Martínez-González C.L., Mercado-Zúñiga C. et al.* // Comput. Mater. Sci. 2022. V. 201. P. 110939. https://doi.org/10.1016/j.commatsci.2021.110939
27. *Eliseev A.A., Yashina L.V., Brzhezinskaya M.M. et al.* // Carbon. 2010. V. 48. P. 2708. https://doi.org/10.1016/j.carbon.2010.02.037
28. *Baldoni M., Leoni S., Sgamellott A.I. et al.* // Small. 2007. V. 3. P. 1730. https://doi.org/10.1002/smll.200700296
29. *Kumar S., Nehra M., Kedia D. et al.* // Prog. Energy Combust. Sci. 2018. V. 64. P. 219. https://doi.org/10.1016/j.pecs.2017.10.005
30. *Gottlieb I.Yu., Ivanov-Shits A.K., Murin I.V. et al.* // Inorgan. mater. 2010. V. 46. P. 1509.
31. *Gotlib Yu., Ivanov-Schitz A. K., Murin I. V. et al.* // Solid State Ionics. 2011. V. 188. P. 6. https://doi.org/10.1016/j.ssi.2010.11.020
32. *Yu. Gotlib, A. K. Ivanov-Schitz, I. V. Murin*. Phys. Solid State. 2011. V. 53. P.2375. https://doi.org/10.1134/S1063783411110126
33. *Gotlib I.Yu., Ivanov-Schitz A.K., Murin I.V. et al.* // J. Phys. Chem. C. 2012. V. 116. P. 19554. https://doi.org/10.1021/jp305518t
34. *Gotlib I.Yu., Ivanov-Schitz A. K., Murin I. V., et al.* // Phys. Solid State. 2014. V.56. P.1472. https://doi.org/10.1134/S1063783414070166
35. *Uvarov N.F.* Composite solid electrolytes. Novosibirsk: Publishing house of the Siberian Branch of the RAS. 2008. 258 p.
36. *Petrov A.V., Salamatov M.S., Ivanov-Schitz A.K. et al.* // Ionics. 2021. V. 27. P. 1255. https://doi.org/10.1007/s11581-020-03710-6
37. *Petrov A.V., Murin I.V., Ivanov-Shits A.K.* // Journal of general chemistry. 2017. V. 87. P. 1062.
38. *Mekky H.* Preprint. https://doi.org/10.21203/rs.3.rs-3951310/v1
39. *Rappé A.K., Casewit C.J., Colwell K.S. et al.* // J. Am. Chem. Soc. 1992. V. 114. P. 10024. https://doi.org/10.1021/ja00051a040